1H and 13C MAS NMR Evidence for Pronounced Ligand-Protein Interactions Involving the Ionone Ring of the Retinylidene Chromophore in Rhodopsin

Creemers, A.F.L.; Kiihne, S.R.; Bovee-Geurts, P.; Grip, W.J. de; Lugtenburg, J.; Groot, H.J.M. de

^{1}H and ^{13}C MAS NMR evidence for pronounced ligand–protein interactions involving the ionone ring of the retinylidene chromophore in rhodopsin

Alain F. L. Creemers*, Suzanne Kiihne*, Petra H. M. Bovee-Geurts†, Willem J. DeGrip*†, Johan Lugtenburg*, and Huub J. M. de Groot*‡

*Leiden Institute of Chemistry, Leiden University, P.O. Box 9502, 2300 RA, Leiden, The Netherlands; and †Department of Biochemistry, Nijmegen Center for Molecular Life Sciences, University of Nijmegen, P.O. Box 9101, 6500 HB, Nijmegen, The Netherlands

Edited by Peter B. Dervan, California Institute of Technology, Pasadena, CA, and approved March 28, 2002 (received for review December 17, 2001)

Rhodopsin is a member of the superfamily of G-protein-coupled receptors. This seven α-helix transmembrane protein is the visual pigment of the vertebrate rod photoreceptor cells that mediate dim light vision. In the active binding site of this protein the ligand or chromophore, 11-*cis*-retinal, is covalently bound via a protonated Schiff base to lysine residue 296. Here we present the complete ^{1}H and ^{13}C assignments of the 11-*cis*-retinylidene chromophore in its ligand-binding site determined with ultra high field magic angle spinning NMR. Native bovine opsin was regenerated with 99% enriched uniformly ^{13}C-labeled 11-*cis*-retinal. From the labeled pigment, ^{13}C carbon chemical shifts could be obtained by using two-dimensional radio frequency-driven dipolar recoupling in a solid-state magic angle spinning homonuclear correlation experiment. The ^{1}H chemical shifts were assigned by two-dimensional heteronuclear (^{1}H-^{13}C) dipolar correlation spectroscopy with phase-modulated Lee–Goldburg homonuclear ^{1}H decoupling applied during the t_1 period. The data indicate nonbonding interactions between the protons of the methyl groups of the retinylidene ionone ring and the protein. These nonbonding interactions are attributed to nearby aromatic acid residues Phe-208, Phe-212, and Trp-265 that are in close contact with, respectively, H-16/H-17 and H-18. Furthermore, binding of the chromophore involves a chiral selection of the ring conformation, resulting in equatorial and axial positions for CH_3-16 and CH_3-17.

Rhodopsin is the photosensitive protein of the rod photoreceptor in the vertebrate retina that mediates dim light vision. Rhodopsin represents a paradigm for the large and diverse family of the G protein-coupled membrane receptors (GPCRs) (1). The GPCRs play an essential role in the transduction of signals from the extracellular environment across the plasma membrane to the interior of every cell type and thus represent an important target for pharmacological intervention (1). Rhodopsin consists of 348-aa residues arranged in seven transmembrane α-helices that span the disk membranes of the rod outer segment (2–4). The chromophore of rhodopsin is an 11-*cis*-retinylidene prosthetic group that is bound to the protein via a protonated Schiff base (pSB) linkage to amino acid residue Lys-296 (Fig. 1*A*) (5). The trigger for photoreceptor activation is the light-induced isomerization of the 11-*cis*-retinylidene ligand to the *all-trans* configuration.

The chromophore of rhodopsin has been studied extensively during the past decades by a variety of techniques. Solid-state ^{13}C magic angle spinning (MAS) NMR spectroscopy has been used in the past to resolve essential details of the spatial and electronic structure of the chromophore. These studies have focused on the retinylidene chain by using ^{13}C-labeled retinals and have assigned the chemical shifts for the polyene carbon atoms (6–12).

Recently, a 10-fold ^{13}C-labeled 11-*cis*-retinal was incorporated in the active site of rhodopsin (12). With solid-state two-dimensional (2D) correlation spectroscopy, detailed information on the electronic structure of the end part of the polyene near the pSB was obtained. Analysis of the NMR data showed that the excess positive charge from the pSB is partially delocalized into the polyene chain, yielding a polaronic conjugation defect close to the nitrogen of the Schiff base (12, 14). This finding demonstrates the utility of multispin labeling in combination with solid-state 2D correlation spectroscopy for the study of ligand–protein interactions for GPCRs.

In the present study uniformly ^{13}C-labeled 11-*cis*-retinal is reconstituted into native opsin in the natural membrane environment, enabling a comprehensive ^{1}H and ^{13}C NMR assay of the electronic structure of the chromophore in the active site of the protein. The ^{1}H and ^{13}C shifts of the ionone ring methyl groups are strongly perturbed by close contacts with the protein environment. The results are discussed in the context of recently established structural models of the chromophore binding pocket.

Materials and Methods

Uniformly ^{13}C-labeled retinal was prepared by total synthesis, starting from commercially available 99% enriched $^{13}C_2$-acetonitrile, $^{13}C_3$-acetone, $^{13}C_2$-acetic acid, [2-^{13}C]-acetic acid, and [1,2,3,4-$^{13}C_4$]-ethyl acetoacetate (15). The 11-*cis*-retinal was obtained by a standard illumination and HPLC purification procedure (9). All subsequent manipulations with the purified 11-*cis* isomer and rhodopsin were performed in the dark or under dim red light conditions with $\lambda > 620$ nm. Opsin was isolated from fresh cattle eyes and reconstituted with the uniformly ^{13}C-labeled 11-*cis*-retinal according to standard procedures (16). The resulting A_{280}/A_{500} ratio of 1.9 ± 0.1 showed that the efficiency of the regeneration was better than 95% (17).

NMR spectra were acquired at 750-MHz ^{1}H frequency (Bruker, Karlsruhe, Germany). The sample was cooled to 223 K, and the MAS spin rate was 12 kHz for all experiments. The spectra were recorded by using 2.0-ms ramped cross polarization and two-pulse phase modulation decoupling during acquisition (18, 19). Radio frequency-driven dipolar recoupling correlation spectra were acquired by using a pathway-selective phase cycling method (20). The 2D heteronuclear correlation spectra were obtained with phase-modulated Lee–Goldburg decoupling during the t_1 period (21, 22).

This paper was submitted directly (Track II) to the PNAS office.

Abbreviations: GPCR, G protein-coupled receptor; pSB, protonated Schiff base; MAS, magic angle spinning; 2D, two-dimensional; $\Delta\sigma^{H}_{lig}$, proton NMR ligation shift; $\Delta\sigma^{C}_{lig}$, carbon NMR ligation shift; $\Delta\bar{\sigma}^{H}_{lig}$, normalized proton NMR ligation shift; $\Delta\bar{\sigma}^{C}_{lig}$, normalized carbon NMR ligation shift; σ^{H}_{lig}, isotropic proton shift of chromophore; σ^{C}_{lig}, isotropic carbon shift of chromophore; σ^{H}_{pSB}, isotropic proton shift of pSB model compound; σ^{C}_{pSB}, isotropic carbon shift of pSB model compound.

‡To whom reprint requests should be addressed. E-mail: ssnmr@chem.leidenuniv.nl.

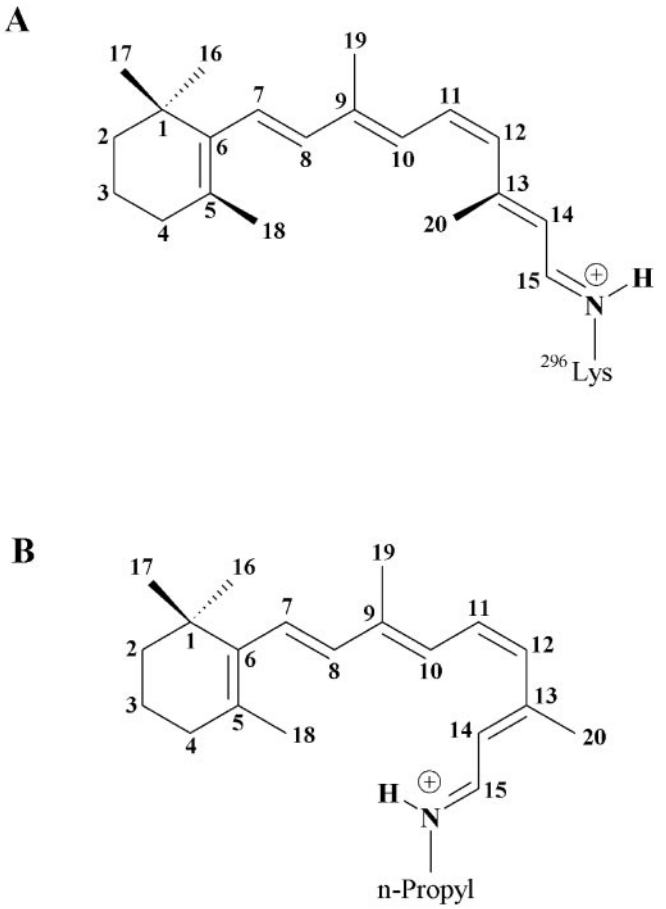

Fig. 1. Molecular structure and International Union of Pure and Applied Chemistry numbering of the 11-*cis*-12-s-*trans*-retinylidene chromophore in rhodopsin (*A*) and the 11-*cis*-12-s-*cis*-retinylidene pSB model (*B*).

^{1}H and ^{13}C chemical shifts of the ligand are reported relative to tetramethylsilane, using the ^{1}H and ^{13}C chemical shift assignments of the phospholipids that are present in the rhodopsin sample as an internal reference (23, 24). In the 2D MAS heteronuclear correlation spectrum, the C═C carbons of the phospholipid acyl chain are easily resolved from the C-10 chromophore response. Based on a global comparison of solid- and solution-state NMR data for lipids, we assign this lipid peak to isotropic proton and carbon shifts of 5.3 ppm and 128.7 ppm, respectively. The lipid methylenic ^{13}C is clearly resolved at 28.7 ppm (7, 12). The associated phospholipid methylenic proton response at 2.7 ppm was used to calculate a Lee Goldburg scaling factor of 0.610, which is in line with the theoretical value of $1/\sqrt{3} = 0.577$ (25).

To calculate the $\Delta\sigma^{C}_{lig}$ (carbon NMR ligation shift) and $\Delta\sigma^{H}_{lig}$ (proton NMR ligation shift) for the polyene region, shifts reported for the pSB model *N*-(11-*cis*-12-s-*cis*-retinylidene)-n-propyliminium trifluoro acetate dissolved in $CDCl_3$ were used (26). Both σ^{H}_{pSB} (isotropic proton shift of pSB model compound) and σ^{C}_{pSB} (isotropic carbon shift of pSB model compound) of this model compound were published, whereas only the σ^{C}_{pSB} are reported for the *N*-(11-*cis*-12-s-*cis*-retinylidene)-n-propyliminium chloride that was used as a reference in our prior investigations (12). The σ^{H}_{pSB} of the ring methylene protons of the 11-*cis*-retinylidene pSB model has not been reported. Because there is ample experimental evidence that in free retinylidene compounds the chemical shifts of these protons are insensitive to the configuration of the C11═C12 bond, an *all-trans*-retinylidene pSB model, *N*-(*all-trans*-12-s-*cis*-retinylidene)-n-butyliminium triflate, was used to estimate the $\Delta\sigma^{H}_{lig}$ of the ring methylene protons (27–29).

Normalization of the $\Delta\sigma^{H}_{lig}$ and $\Delta\sigma^{C}_{lig}$ is based on the difference of the proton and carbon chemical shift scale. The protons have a chemical shift dispersion of ≈15 ppm whereas the carbon response has a much larger range of ≈200 ppm. Scaling according to $\Delta\tilde{\sigma}^{H}_{lig}$ (normalized proton NMR ligation shift) = $\Delta\sigma^{H}_{lig}/15$ and $\Delta\tilde{\sigma}^{C}_{lig}$ (normalized carbon NMR ligation shift) = $\Delta\sigma^{C}_{lig}/200$ provides a normalized image that is useful to compare proton and carbon NMR ligation shifts.

Results

The one-dimensional ^{13}C cross polarization/MAS spectra from rhodopsin membranes containing either the uniformly ^{13}C-labeled or the unlabeled 11-*cis*-retinylidene chromophore are shown in Fig. 4, which is published as supporting information on the PNAS web site, www.pnas.org. Several narrow signals, from methyl and methylene ^{13}C in the ionone ring of the chromophore, are detected in the aliphatic region (5–40 ppm) of the spectrum. In the vinylic region (120–150 ppm) the resonances of the carbon labels in the polyene chain can be identified. The response at σ^{C}_{lig} (isotropic carbon shift of chromophore) = 127.9 ppm is superimposed on the broad natural abundance signal around ≈130 ppm of the unsaturated carbon atoms of the phospholipid acyl chains and the aromatic side chains of the protein. Two signals with σ^{C}_{lig} = 168.3 ppm and σ^{C}_{lig} = 165.8 ppm with corresponding spinning side bands at σ^{C}_{lig} = 103.9 ppm and σ^{C}_{lig} = 101.4 ppm are from vinylic carbon atoms that are shifted downfield because of a relatively high positive atomic charge density. Finally, the broad signal at σ^{C}_{lig} = 175 ppm is caused by the carbonyl moieties of peptide bonds and lipid ester groups.

In the composite Fig. 2, contour regions from 2D homonuclear (^{13}C-^{13}C) and 2D heteronuclear (^{1}H-^{13}C) dipolar correlation spectra of the rhodopsin containing the uniformly ^{13}C-labeled chromophore are shown. The network of nearest-neighbor correlation signals is indicated in the plot with pairs of regular numbers. The correlations between carbon nuclei of the molecular frame C_1–C_{15} are indicated with solid lines in the corresponding panels of the 2D radio frequency-driven dipolar recoupling spectrum. Furthermore, correlations between the carbon atoms of the molecular frame and the directly attached methyl groups are shown with dashed lines.

Even for the relatively short mixing time of 1.23 ms that was used for the radio frequency-driven dipolar recoupling experiment, relayed transfer along the ^{13}C-labeled network gives rise to additional correlations, which are indicated in Fig. 2 with italic numbers. In particular, the methyl groups of the chromophore show relayed correlations with vinylic carbon atoms. The longer-range correlations are generally weaker than the nearest-neighbor correlations. An exception is the relatively strong long-range correlation between carbon C-4 of the ionone ring and CH_3-18. Its signal is superimposed on a broad and weak cross peak of C-3 and C-4.

The 2D ^{13}C dataset leads to a complete assignment of the ^{13}C responses of the chromophore (Table 1). The σ^{C}_{lig} for the polyene chain correspond with the assignments reported by Smith *et al.* (7) and Verhoeven *et al.* (12) within the experimental errors of 0.4 and 0.6 ppm, respectively. This finding validates the procedure of calibrating the ^{13}C shift scale by using the lipid response. The ^{13}C assignment can be used for an assignment of the proton signals from the chromophore bound to its receptor target in the natural membrane environment. High-field ^{1}H-^{13}C heteronuclear correlation data from the rhodopsin containing the uniformly ^{13}C-labeled chromophore are shown in the bottom of Fig. 2. These data were collected with a short cross polarization contact time of 50 μs to excite predominantly heteronuclear correlations between ^{13}C nuclei and directly bound protons. For

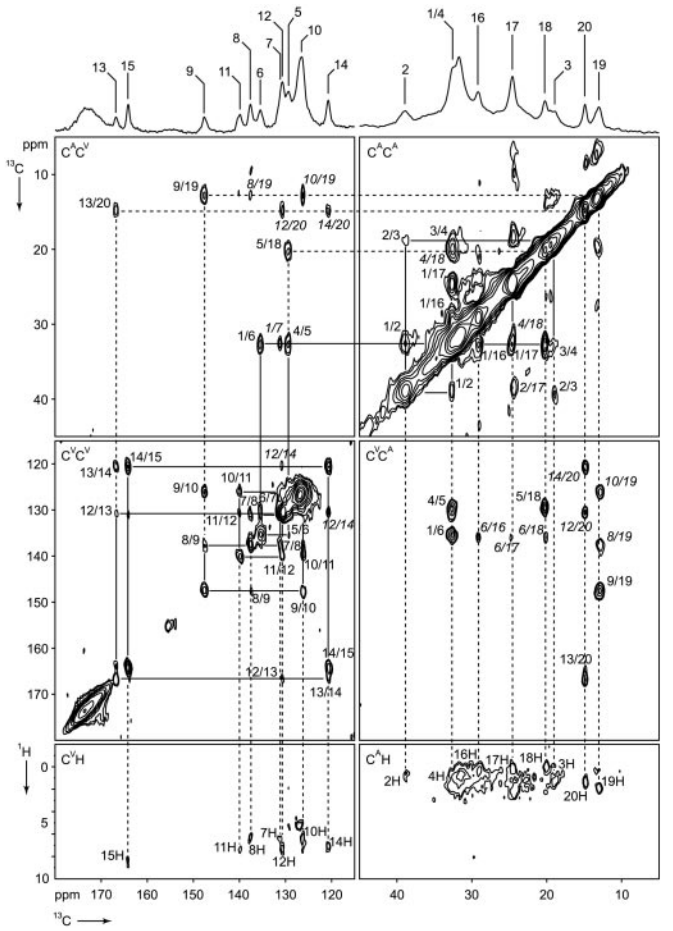

Fig. 2. Contour regions of the 2D homonuclear (^{13}C-^{13}C) and 2D heteronuclear (^{1}H-^{13}C) dipolar correlation spectra of the uniformly ^{13}C-labeled retinylidene in rhodopsin. The regions shown in the *Top Left* (C^AC^V) and *Middle Right* (C^VC^A) display correlations between vinylic and aliphatic carbon nuclei. Correlations between vinylic ^{13}C are in the *Middle Left* (C^VC^V), couplings between aliphatic ^{13}C are revealed in the *Top Right* (C^AC^A). (*Bottom*) The correlations between protons and vinylic (C^VH) or aliphatic (C^AH) ^{13}C are shown.

most heteronuclear correlation signals, the high resolution in the carbon dimension is sufficient to assign the corresponding isotropic proton shifts of the chromophore ($\sigma_{lig}{}^{H}$, Table 2). The aliphatic region of the 2D ^{1}H-^{13}C spectrum (C^AH) is complicated because of strong overlap with correlations involving protons attached to carbons of phospholipid and protein. A 2D ^{1}H-^{13}C heteronuclear correlation spectrum of natural abundance rhodopsin was therefore collected to identify the ''background'' signals (data not shown).

Discussion

By comparing the shifts for the chromophore in rhodopsin with the responses collected from model compounds, an NMR assay of the spatial and electronic structure of the chromophore can be obtained (12). The $\Delta\sigma_{lig} = \sigma_{lig} - \sigma_{pSB}$ are listed in Tables 1 and 2 for the ^{13}C and the ^{1}H responses, respectively. The $\Delta\sigma_{lig}$ reflect differences in the electronic and spatial molecular structure between the pSB model compound and the chromophore bound in the active site of the protein. They can be used as a probe for ligand–protein interactions between the chromophore and the protein binding pocket, including protein-induced conformational restraints in the ligand or electronic effects on the chromophore exerted by the protein.

Table 1. The complete carbon assignment $\sigma_{lig}{}^{C}$ of the 11-*cis*-retinylidene chromophore of rhodopsin compared with $\sigma_{pSB}{}^{C}$ for *N*-(11-*cis*-retinylidene)-n-propyl-iminium trifluoro acetate in solution to obtain the $\Delta\sigma_{lig}{}^{C}$

Position	$\sigma_{lig}{}^{C}$, ppm	$\sigma_{pSB}{}^{C}$, ppm*	$\Delta\sigma_{lig}{}^{C}$, ppm
C-1	34.0	34.1	−0.1
C-2	40.3	38.9	1.4
C-3	20.3	18.8	1.5
C-4	34.0	33.0	1.0
C-5	130.9	132.1	−1.2
C-6	137.0	137.2	−0.2
C-7	132.8	132.3	0.5
C-8	139.1	137.2	1.9
C-9	149.0	147.8	1.2
C-10	127.9	126.4	1.5
C-11	141.4	138.7	2.7
C-12	132.2	128.7	3.5
C-13	168.3	165.8	2.5
C-14	122.3	120.5	1.8
C-15	165.8	163.3	2.5
C-16	30.6	28.9	1.7
C-17	26.1	28.9	−2.8
C-18	21.7	22.1	−0.4
C-19	14.4	12.6	1.8
C-20	16.3	18.8	−2.5

*Data from Shriver *et al.* (26).

It has been shown that $\Delta\sigma_{lig}^{C}$ can be quite informative when considered at the molecular level and reveal systematic variations in the bound ligand (12). In comparison, $\Delta\sigma_{lig}^{H}$ is even more sensitive in providing information about nonbonding interactions between the chromophore and the protein. A $\Delta\sigma_{lig}^{H} \geq 0.5$ ppm can be considered highly significant on the proton shift scale of ≈15 ppm. Thus the combination of $\Delta\sigma_{lig}^{C}$ and $\Delta\sigma_{lig}^{H}$ can give comprehensive information about localized nonbonding interactions between ligand and receptor.

Fig. 3*A* provides a visual representation of the $\Delta\sigma_{lig}^{C}$ and $\Delta\sigma_{lig}^{H}$ of the chromophore in rhodopsin. The color-encoded NMR ligation shift patterns can be used for a discussion of local protein–ligand interactions. In addition, the scaled $\Delta\tilde{\sigma}_{lig}^{C}$ and $\Delta\tilde{\sigma}_{lig}^{H}$ provide a view of the relative magnitude of the ^{13}C and ^{1}H

Table 2. The complete proton assignment $\sigma_{lig}{}^{H}$ of the 11-*cis*-retinylidene chromophore in rhodopsin

Position	$\sigma_{lig}{}^{H}$, ppm	$\sigma_{pSB}{}^{H}$, ppm	$\Delta\sigma_{lig}{}^{H}$, ppm
H-2	1.0	1.49*	−0.5
H-3	1.6	1.63*	0.0
H-4	1.0	2.06*	−1.1
H-7	6.4	6.55†	−0.2
H-8	6.2	6.36†	−0.2
H-10	6.4	6.98†	−0.6
H-11	7.2	7.12†	0.1
H-12	7.2	6.31†	0.9
H-14	7.0	6.71†	0.3
H-15	8.1	9.19†	−1.1
H-16	0.8	1.05†	−0.3
H-17	0.6	1.05†	−0.5
H-18	0.5	1.73†	−1.2
H-19	2.2	2.14†	0.1
H-20	1.7	2.57†	−0.9

The $\Delta\sigma_{lig}{}^{H}$ are calculated from $\sigma_{lig}{}^{H}$ minus $\sigma_{pSB}{}^{H}$ as described in the text.
*Data from Elia *et al.* (29).
†Data from Shriver *et al.* (26).

CHEMISTRY

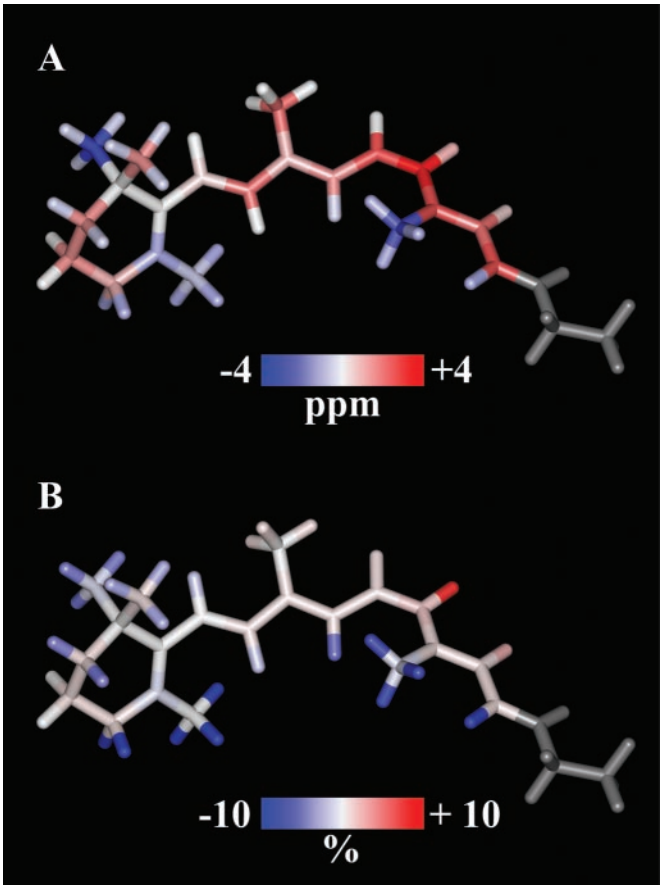

Fig. 3. Visual representation of (*A*) the $\Delta\sigma^{C}_{lig}$ and $\Delta\sigma^{H}_{lig}$ NMR ligation shifts in Tables 1 and 2 and (*B*) normalized $\Delta\tilde{\sigma}^{C}_{lig}$ and $\Delta\tilde{\sigma}^{H}_{lig}$. The model corresponds with the image of the ground state structure calculated with Carr–Parrinello molecular dynamics (10, 14). Blue and red colors reflect the upfield and downfield $\Delta\sigma_{lig}$, respectively, and the larger the shift the darker the color.

effects and an overview of significant ligand–protein interactions acting on the chromophore bound in the active site of the protein (Fig. 3*B*).

Charge Delocalization in the Polyene Chain of the 11-*cis*-Retinylidene Chromophore. Previous experiments already revealed downfield $\Delta\sigma^{C}_{lig}$ for the C10–C15 region in the tail end of the polyene chain of the retinylidene in rhodopsin in comparison with *N*-(11-*cis*-retinylidene)-n-propyliminium chloride (12). The $\Delta\sigma^{C}_{lig}$ was ascribed to three synergistic contributions leading to an excess of positive charge in the polyene: (*i*) the electronegative nitrogen, (*ii*) the protonation, and (*iii*) the counterion strength. The color-encoded data in Fig. 3*A* show a similar pattern for the $\Delta\sigma^{C}_{lig}$ of the vinylic carbon nuclei in the tail end of the polyene chain of the chromophore, with the largest downfield shift for C-12, $\Delta\sigma^{C}_{lig}$ = 3.5 ppm (Table 1).

The stronger positive charge delocalization into the rhodopsin polyene compared with the model compounds is thought to be caused by electrostatic interactions with polar or negatively charged side chains of amino acid residues that are in close contact with the tail end of the polyene (30–32). Based on earlier solid-state NMR studies on ^{15}N-Lys-labeled rhodopsin, an effective center-to-center distance between the counterion and the pSB nitrogen of 0.43 ± 0.01 nm was estimated (33, 34). This effective radius is larger than the 0.34 nm derived from the recently published crystal structure and implies the presence of a complex counterion (3, 4). Such a complex counterion could be organized around a hydrogen-bonded network positioning a water molecule between the positively charged nitrogen of the pSB and the negatively charged carboxylate of Glu-113 (34). Several studies showed that upon addition of D_2O the proton of the pSB exhibits rapid H-D exchange already in the dark, indicating that the Schiff base region is easily accessible for bulk water molecules (35, 36).

The Palczewski model shows another glutamic acid residue, Glu-181, in the second extracellular loop, and a tyrosine residue, Tyr-268, in transmembrane helix VI, to be in close contact with the tail end of the polyene (3, 4). Site-directed mutagenesis studies of either residue leads to significant shifts in the spectral properties of the pigment (37, 38). Therefore, similar to Glu-113, Glu-181 and Tyr-268 may be involved in modulating the positive charge delocalization in the polyene, resulting in the observed large downfield $\Delta\sigma^{C}_{lig}$ of the carbon resonances in the tail end of the polyene chain. In addition, these two amino acid residues might contribute to a hydrogen-bonded network. *Ab initio* molecular dynamics simulations provided evidence that the ^{13}C shifts of the carbons of the tail end of the polyene are sensitive to the position of the counterion (30). These simulations also suggest that other charged residues that are located in the vicinity of the C10-C13 region, like Glu-181 and Tyr-268, may contribute to the observed downfield $\Delta\sigma^{C}_{lig}$.

Conformation of the 11-*cis*-Retinylidene Chromophore. By using a uniformly ^{13}C-labeled chromophore, the assay of the charge delocalization is extended to the ring end of the polyene. In the past, NMR studies with 5-^{13}C-labeled *all-trans*-retinal reconstituted into bacteriorhodopsin have demonstrated that the counterion strength affects the shift of carbon C-5 in the ionone ring of the chromophore (39, 40). This finding contrasts with the data for rhodopsin, because the charge delocalization appears to be restricted to the region between carbon C-7 and C-15 (Fig. 3*A*). The difference between the two retinal proteins may be related to the conformation of the C6–C7 single bond. At an early stage it was established with MAS NMR shift tensor measurements using rhodopsin reconstituted with ^{13}C-5-labeled retinal and retinoic acid model compounds that the 6–7 single bond has a 6-s-*cis* conformation in rhodopsin, which is different from the 6-s-*trans*-retinylidene chromophore in bacteriorhodopsin (7).

Recent deuterium MAS experiments on oriented rhodopsin preparations have been interpreted in terms of a 6-s-*trans* conformation of the chromophore (41). In contrast, the x-ray data point to a 6-s-*cis* structure, but the resolution is insufficient to rule out the possibility of a mixture of 6-s-*cis* and 6-s-*trans* (4). MAS NMR chemical shifts have been shown to be a sensitive indicator of this bond conformation, and our shifts match those of the previous MAS NMR study, thus reconfirming the 6-s-*cis* conformation (7, 39). Additionally, as can be seen in Fig. 2, there is no evidence of signal doubling or splitting and therefore the ring conformation must be unique.

In the past, NMR studies have provided convincing evidence for a conformational change leading to a nonplanar C10–C13 segment for the polyene chain in the chromophore relative to the models in solution (Fig. 1) (9, 10). Because the 12-s-*cis* conformation is energetically favorable over the 12-s-*trans*, the equilibrium will be shifted in solution toward 12-s-*cis* (Fig. 1*B*) (42). In the protein, however, there is a nonplanar 12-s-*trans* conformation (Fig. 1*A*) (4, 10, 43). Also the most recent refined x-ray model for rhodopsin includes an out-of-plane distortion in the C_{10}–C_{13} segment with a dihedral angle for C_{10}–C_{11}–C_{12}–C_{13} of $\varphi = 7.9°$ (4). This distortion is in line with the torsional angle of C_{10}–C_{11}–C_{12}–C_{13} of $\varphi = 17°$, which was calculated from the NMR distance constraints with Carr–Parrinello molecular dynamics (44). The out-of-plane distortion is distributed over several bonds (10).

The ^{1}H shift data provide additional qualitative support for a

conformational change involving the C10–C13 segment of the chromophore by binding to the protein, because the σ^{H}_{lig} of the 12-s-*trans* chromophore in rhodopsin is different from the σ^{H}_{pSB} of the pSB model in the 12-s-*cis* conformation in solution.

The downfield $\Delta\tilde{\sigma}^{H}_{lig}$ of H-12 and H-14 may be caused by a reduced intramolecular steric interaction between CH_3-20 and the nearby protons H-12 and H-14, relative to the pSB model. In addition, the upfield $\Delta\tilde{\sigma}^{H}_{lig}$ of H-10 and H-20 may reflect the steric interaction between H-10 and the methyl group C-20 in the 11-*cis*-12-s-*trans*-retinylidene chromophore bound to the protein, which is released in the free 12-s-*cis* conformation. Furthermore, the observed upfield $\Delta\sigma^{C}_{lig} = -2.5$ ppm of CH_3-20 is in line with a distorted s-*trans* conformation of the 12-s bond. Addition of a methyl group at C-10, giving 10-methylrhodopsin, yields a larger out-of-plane distortion in the isomerization region compared with rhodopsin and an additional upfield $\Delta\sigma^{C}_{lig} = -1.6$ ppm compared with the C-20 response in rhodopsin (10, 45, 46). This finding suggests a correlation between torsion and the ^{13}C-20 shift. Finally, a relatively large $\Delta\sigma^{H}_{lig} = -1.1$ ppm is detected for the H-15. This $\Delta\sigma^{H}_{lig}$ may be produced by a difference in the conformation around the C14–C15 bond between the 11-*cis*-retinylidene chromophore and the pSB model compound or by an interaction with a nearby protein residue (3, 4, 33, 34).

The absence of conformational shifts for C-7, C-8, and C-19 provides strong evidence for a highly similar electronic and spatial conformation of the rhodopsin chromophore and the pSB model. In particular, Fourier transform IR and resonance Raman spectroscopic studies have been interpreted in terms of a close contact between the C-19 methyl group and the surrounding protein (47, 48). Although these studies indicate strong ligand–protein interactions for CH_3-19, it is clear from the NMR that the protein has no significant effect on the conformation of the chromophore around C-19.

Finally, both methyl groups C-16 and C-17 of the pSB model compound in solution resonate with $\sigma^{C}_{pSB} = 28.9$ ppm (26). These methyl groups have significantly different shifts in rhodopsin (54). One methyl group is detected with $\sigma^{C}_{lig} = 26.1$ ppm, corresponding with a $\Delta\sigma^{C}_{lig}$ of -2.8 ppm, whereas the other resonates with $\sigma^{C}_{lig} = 30.6$ ppm, a $\Delta\sigma^{C}_{lig}$ of $+1.7$ ppm. In contrast, the $\Delta\sigma^{H}_{lig} = -0.5$ ppm and -0.3 ppm for the protons of these two methyl groups are both upfield and of comparable magnitude.

The single resonance of CH_3-16 and CH_3-17 of the pSB model compound in solution is caused by motional averaging between the equatorial and axial conformation for the two methyl groups attached to the sp^3-hybridized C-1 of the six-membered ring (49). Evidently the protein prevents the ring flip that occurs in solution. In this way, our data contribute to converging evidence that the chromophore conformation is unique with an equatorial position for CH_3-16 and an axial CH_3-17 methyl caused by the steric constraints from the protein binding pocket (54). The relatively large upfield $\Delta\sigma^{C}_{lig}$ of C-17 can be explained in terms of a γ effect caused by steric hindrance between the protons of C-17 and H-3 (50, 54). Because the CH_3-16 occupies an equatorial position, it experiences weaker steric interactions than in the pSB model in solution, which can explain the observed downfield NMR ligation shift.

NMR Ligation Shifts in the Ionone Moiety of the Chromophore Indicate Pronounced Interactions with the Protein Environment. Binding studies on rhodopsin using acyclic retinal analogs have shown that the ionone moiety plays a central role in the formation of a stable photoactive pigment. In particular, the methyl groups attached to the ring appear to be essential for binding (51). Reconstitution studies have provided evidence for specific protein–ligand interactions, which are essential for correct positioning of the ionone ring and in particular the methyl groups. The complete proton and carbon assignments of the ionone moiety of the chromophore provide a view on the molecular details of these interactions with atomic selectivity.

In particular, the proton shifts of the ligand can reveal the presence of aromatic side chains in the binding pocket. Calculations of ring current intensities demonstrate that an extension of the delocalization of electrons in an aromatic system produces an increase of the magnitude of the ring current effect that leads to upfield proton shifts (52). These ring current effects can become highly significant on the proton shift scale of ≈15 ppm. The $\Delta\tilde{\sigma}^{H}_{lig}$ reveal relatively strong ligand–receptor interactions for the ionone ring of the chromophore. The CH_3-18 protons show the largest upfield $\Delta\tilde{\sigma}^{H}_{lig}$ observed in the chromophore. The protons of the adjacent carbon C-4 also demonstrate a large upfield $\Delta\tilde{\sigma}^{H}_{lig}$. These relatively large $\Delta\tilde{\sigma}^{H}_{lig}$ indicate the presence of a tryptophan amino acid residue (52). Earlier studies already suggested that a tryptophan residue should be located in the vicinity of the ionone ring (13, 53). Based on these studies and the recently published x-ray model, a tryptophan residue at a distance of ≈3.8 Å to C-18, Trp-265 in transmembrane helix VI, is most likely responsible for these interactions (3, 4). The $\Delta\tilde{\sigma}^{H}_{lig}$ for the CH_3-16 and CH_3-17 can be explained in terms of ring current effects from two nearby phenylalanine side chains, Phe-208 and Phe-212 of transmembrane helix V (3, 44, 52). According to the x-ray model, Phe-212 is also located close to the methylene protons attached to C-2 (≈4 Å), which is in line with the observed upfield $\Delta\tilde{\sigma}^{H}_{lig}$ for the C-2 protons. In this way the NMR data contribute to converging evidence that nonbonding interactions between the methyl groups and the nearby phenylalanines contribute to the ''scaffolding'' of the protein structure and the retinylidene binding pocket.

Other parts of the ionone moiety appear less important for binding to the protein. The carbon responses of C-2 and C-3 are relatively broad, which indicates disorder of this part of the ring. This finding correlates with ligand analog experiments, which demonstrated that acyclic retinal analogs could bind as well. It also suggests that C-2 and C-3 play only a modest part in rhodopsin–ligand recognition in the dark inactive state of the receptor (51).

It is difficult to attribute the small $\Delta\tilde{\sigma}^{C}_{lig}$ to a specific mechanism. For instance, C-5 shows a small upfield $\Delta\sigma^{C}_{lig} = -1.2$ ppm, with $\Delta\tilde{\sigma}^{C}_{lig} = -0.4$ ppm for the adjacent CH_3-18. The x-ray model and rotational resonance solid-state MAS NMR studies demonstrate that the C5–C8 segment has a twisted out-of-plane conformation (3, 4, 54). *Ab initio* calculations on pSB models suggested that the C5═C6 bond and the adjacent methyl group C-18 lie in one plane (42). Conformational distortions might be the origin of the observed small $\Delta\tilde{\sigma}^{C}_{lig}$ for C-5 and C18. In addition, the x-ray model of rhodopsin indicates that the carboxylic group of a glutamic acid residue, Glu-122, is in close contact to C-5 (≈3.8 Å) (3, 4). Interaction with the side chain of such a polar amino acid could also result in a small upfield $\Delta\sigma^{C}_{lig}$.

Conclusions

High-field solid-state 2D homonuclear and 2D heteronuclear MAS NMR dipolar correlation spectroscopy on rhodopsin reconstituted with a uniformly ^{13}C-labeled 11-*cis*-retinylidene chromophore provided a complete ^{13}C and ^{1}H chemical shift assignment for the chromophore. The $\Delta\sigma_{lig}$ and $\Delta\tilde{\sigma}_{lig}$ reflect the spatial and electronic structure of the chromophore in the active site of rhodopsin relative to the pSB model in solution and thus provide a detailed view on the mechanisms of ligand–protein interactions with atomic selectivity.

Pronounced $\Delta\tilde{\sigma}^{H}_{lig}$ are observed for the methyl protons of the ring moiety. The data provide converging evidence for nonbonding interactions between the chromophore and the protein binding pocket involving the aromatic amino acid residues Phe-208, Phe-212, and Trp-265 that are in close contact with

H-16/H-17 and H-18, respectively. The $\Delta\tilde{\sigma}^{H}_{lig}$ in the polyene chain and the relatively large downfield $\Delta\sigma^{C}_{lig}$ observed for CH_3-20 are consistent with a nonplanar conformation of the 12-s bond. Finally, binding of the chromophore involves chiral selection by fixation of the ring puckering, which results in well-defined axial and equatorial positions for CH_3-17 and CH_3-16.

This study shows that the combination of a uniformly ^{13}C-labeled ligand incorporated into the active binding site of a GPCR with 2D solid-state NMR correlation spectroscopy can provide detailed information about ligand–protein interaction patterns. In this way a solid-state NMR "snapshot" of the spatial and electronic ground state structure of a ligand bound to its GPCR target in the natural membrane is obtained.

We thank J. Hollander, C. Erkelens, and F. Lefeber for assistance with the MAS NMR experiments. Cambridge Isotope Laboratories is gratefully acknowledged for their kind gift of all ^{13}C-labeled starting materials that were used for the preparation of the uniformly ^{13}C-labeled retinal. H.J.M.d.G. is a recipient of a pioneer award of the Chemical Science section of the Netherlands Organization for Research (NWO). The 750-MHz instrumentation was financed in part by Demonstration Project Grant BIO4-CT97-2101 (DG12-SSMI) of the commission of the European Communities.

1. Baldwin, J. M., Schertler, G. F. X. & Unger, V. M. (1997) *J. Mol. Biol.* **272,** 144–164.
2. Unger, V. M., Hargrave, P. A., Baldwin, J. M. & Schertler, G. F. X. (1997) *Nature (London)* **389,** 203–206.
3. Palczewski, K., Kumasaka, T., Hori, T., Behnke, C. A., Motoshima, H., Fox, B. A., Le Trong, I., Teller, D. C., Okada, T., Stenkamp, R. E., *et al*. (2000) *Science* **289,** 739–745.
4. Teller, D. C., Okada, T., Behnke, C. A., Palczewski, K. & Stenkamp, R. E. (2001) *Biochemistry* **40,** 7761–7772.
5. Gärtner, W. (2001) *Angew. Chem. Int. Ed. Engl.* **40,** 2977–2981.
6. Mollevanger, L. C., Kentgens, A. P., Pardoen, J. A., Courtin, J. M., Veeman, W. S., Lugtenburg, J. & de Grip, W. J. (1987) *Eur. J. Biochem.* **163,** 9–14.
7. Smith, S. O., Palings, I., Copié, V., Raleigh, D. P., Courtin, J., Pardoen, J. A., Lugtenburg, J., Mathies, R. A. & Griffin, R. G. (1987) *Biochemistry* **26,** 1606–1611.
8. Smith, S. O., Courtin, J., de Groot, H., Gebhard, R. & Lugtenburg, J. (1991) *Biochemistry* **30,** 7409–7415.
9. Feng, X., Verdegem, P. J. E., Lee, Y. K., Sandström, D., Edén, M., Bovee-Geurts, P., de Grip, W. J., Lugtenburg, J., de Groot, H. J. M. & Levitt, M. H. (1997) *J. Am. Chem. Soc.* **119,** 6853–6857.
10. Verdegem, P. J. E., Bovee-Geurts, P. H. M., de Grip, W. J., Lugtenburg, J. & de Groot, H. J. M. (1999) *Biochemistry* **38,** 11316–11324.
11. de Groot, H. J. M (2000) *Curr. Opin. Struct. Biol.* **10,** 593–600.
12. Verhoeven, M. A., Creemers, A. F. L. Bovee-Geurts, P. H. M., de Grip, W. J., Lugtenburg, J. & de Groot, H. J. M. (2001) *Biochemistry* **40,** 3282–3288.
13. Kochendoerfer, G. G., Kaminaka, S. & Mathies, R. A. (1997) *Biochemistry* **36,** 13153–13159.
14. Buda, F., de Groot, H. J. M. & Bifone, A. (1996) *Phys. Rev. Lett.* **77,** 4474–4477.
15. Lugtenburg, J., Creemers, A. F. L., Verhoeven, M. A., van Wijk, A. A. C., Verdegem, P. J. E., Monnee, M. C. F. & Jansen, F. J. H. M. (1999) *Pure Appl. Chem.* **71,** 2245–2251.
16. DeGrip, W. J., Daemen, F. J. M. & Bonting, S. L. (1980) *Methods Enzymol.* **67,** 301–320.
17. De Grip, W. J. (1982) *Methods Enzymol.* **81,** 197–207.
18. Pines, A., Gibby, M. G. & Waugh, J. S. (1973) *J. Chem. Phys.* **59,** 569–573.
19. Balaban, T. S., Holzwarth, A. R., Schaffner, K., Boender, G. J. & de Groot, H. J. M. (1995) *Biochemistry* **34,** 15259–15266.
20. Boender, G. J., Raap, J., Prytulla, S., Oschkinat, H. & de Groot, H. J. M. (1995) *Chem. Phys. Lett.* **237,** 502–508.
21. Van Rossum, B.-J., Boender, G. J. & de Groot, H. J. M. (1996) *J. Magn. Reson. A* **120,** 274–277.
22. Vinogradov, E., Madhu, P. K. & Vega, S. (1999) *Chem. Phys. Lett.* **314,** 443–450.
23. Brown, M. F., Miljanich, G. P. & Dratz, E. A. (1977) *Proc. Natl. Acad. Sci. USA* **74,** 1978–1982.
24. Zumbulyadis, N. & O'Brien, D. F. (1979) *Biochemistry* **18,** 5427–5432.
25. Van Rossum, B.-J., Förster, H. & de Groot, H. J. M. (1997) *J. Magn. Reson.* **124,** 516–519.
26. Shriver, J. W., Mateescu, G. D. & Abrahamson, E. W. (1979) *Biochemistry* **18,** 4785–4792.
27. Liu, R. S. H. & Asato, A. E. (1984) *Tetrahedron* **40,** 1931–1969.
28. Englert, G. (1995) in *Carotenoids: Spectroscopy*, eds. Britton, G., Liaaen-Jensen, S. & Pfander, H. (Birkhäuser, Basel), Vol. 1B, pp. 163–167.
29. Elia, G. R., Childs, R. F., Britten, J. F., Yang, D. S. C. & Santarsiero, B. D. (1996) *Can. J. Chem.* **74,** 591–601.
30. La Penna, G., Buda, F., Bifone, A. & de Groot, H. J. M. (1998) *Chem. Phys. Lett.* **294,** 447–453.
31. Buda, F., Giannozzi, P. & Mauri, F. (2000) *J. Phys. Chem.* **104,** 9048–9053.
32. Buda, F., Touw, S. I. E. & de Groot, H. J. M. (2001) in *Perspectives on Solid-State NMR in Biology*, eds. Kiihne, S. & de Groot, H. J. M. (Kluwer, Dordrecht, The Netherlands), pp. 111–122.
33. Eilers, M., Reeves, P. J., Ying, W., Khorana, H. G. & Smith, S. O. (1999) *Proc. Natl. Acad. Sci.* USA **96,** 487–492.
34. Creemers, A. F. L., Klaassen, C. H. W., Bovee-Geurts, P. H. M., Kelle, R., Kragl, U., Raap, J., de Grip, W. J., Lugtenburg, J. & de Groot, H. J. M. (1999) *Biochemistry* **38,** 7195–7199.
35. Oseroff, A. R. & Callender, R. H. (1974) *Biochemistry* **13,** 4243–4248.
36. Mathies, R. A., Oseroff, A. R. & Stryer, L. (1976) *Proc. Natl. Acad. Sci. USA* **73,** 1–5.
37. Nakayama, T. A. & Khorana, H. G. (1991) *J. Biol. Chem.* **266,** 4269–4275.
38. Terakita, A., Yamashita, T. & Shichida, Y. (2000) *Proc. Natl. Acad. Sci. USA* **97,** 14263–14267.
39. Harbison, G., Mulder, P., Pardoen, H., Lugtenburg, J., Herzfeld, J. & Griffin, R. G. (1985) *J. Am. Chem. Soc.* **107,** 4809–4816.
40. Hu, J., Griffin, R. G. & Herzfeld, J. (1994) *Proc. Natl. Acad. Sci. USA* **91,** 8880–8884.
41. Gröbner, G., Burnett, I. J., Glaubitz, C., Choi, G., Mason, A. J. & Watts, A. W. (2000) *Nature (London)* **405,** 810–813.
42. Terstegen, F. & Buss, V. (1996) *J. Mol. Struct.* **369,** 53–65.
43. Lin, S. W., Groesbeek, M., van der Hoef, I., Verdegem, P., Lugtenburg, J. & Mathies, R. A. (1998) *J. Phys. Chem. B* **102,** 2787–2806.
44. Bifone, A., de Groot, H. J. M. & Buda, F. (1997) *J. Phys. Chem. B* **101,** 2954–2958.
45. Tonelli, A. E. (1989) *NMR Spectroscopy and Polymer Microstructure: The Conformational Connection* (VCH, Weinheim), pp. 43–53.
46. De Lange, F., Bovee-Geurts, P. H., Van Oostrum, J., Portier, M. D., Verdegem, P. J., Lugtenburg, J. & De Grip, W. J. (1998) *Biochemistry* **37,** 1411–1420.
47. Eyring, G., Curry, B., Mathies, R. A., Fransen, R., Palings, I. & Lugtenburg, J. (1980) *Biochemistry* **19,** 2410–2418.
48. Ganter, U. M., Schmid, E. D., Perez-Sala, D., Rando, R. R. & Siebert, F. (1989) *Biochemistry* **28,** 5954–5962.
49. Breitmaier, E. & Voelter, W. (1987) *Carbon-13 NMR Spectroscopy* (VCH, Weinheim), 3rd Ed., pp. 115–116.
50. Günther, H. (1995) *NMR Spectroscopy* (Wiley, Chichester, U.K.), 2nd Ed., pp. 501–504.
51. Nakanishi, K. & Crouch, R. (1995) *Isr. J. Chem.* **35,** 253–272.
52. Giessner-Prettre, C. & Pullman, B. (1971) *J. Theor. Biol.* **31,** 287–294.
53. Lin, S. W. & Sakmar, T. P. (1996) *Biochemistry* **35,** 11149–11159.
54. Spooner, P. J. R., Sharples, J. M., Verhoeven, M. A., Lugtenburg, J., Glaubitz, C. & Watts, A. (2002) *Biochemistry,* in press.